nature portfolio

https://doi.org/10.1038/s41586-024-08570-y

Supplementary information

Impact of Amazonian deforestation on precipitation reverses between seasons

In the format provided by the authors and unedited

Supporting Information *for*

Impact of Amazonian deforestation on precipitation reverses between seasons

Yingzuo Qin[1], Dashan Wang[1], Alan D. Ziegler[2,3], Bojie Fu[4], Zhenzhong Zeng[1,*]

[1]School of Environmental Science and Engineering, Southern University of Science and Technology, Shenzhen, China

[2]Faculty of Fisheries Technology and Aquatic Resources, Mae Jo University, Chiang Mai, Thailand

[3]Andaman Coastal Research Station for Development, Faculty of Fisheries, Kasetsart University, Ranong, Thailand

[4]State Key Laboratory for Ecological Security of Regions and Cities, Research Center for Eco-Environmental Sciences, Chinese Academy of Sciences, Beijing, China

[*]Corresponding author: Zhenzhong Zeng (zengzz@sustech.edu.cn)

Manuscript for *Nature*

This PDF file includes:

Figures S1 to S17

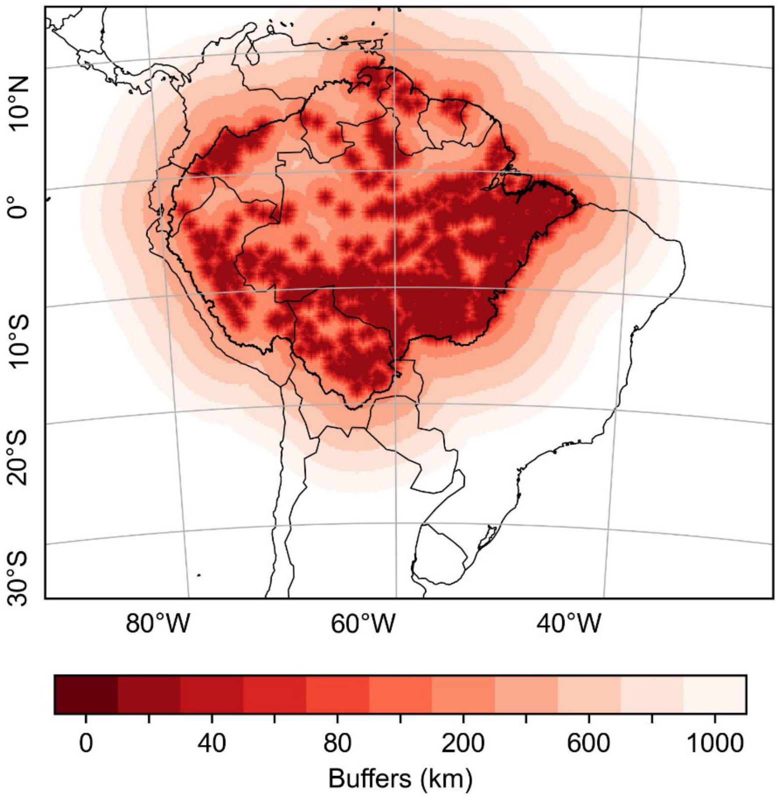

Figure S1. Buffer settings used in modeling results. The 0-km buffer corresponds to the deforested grids. The 20-1,000 km buffers represent all grids within 20-1,000 km of the deforested grids (including the inner buffers and deforested grids).

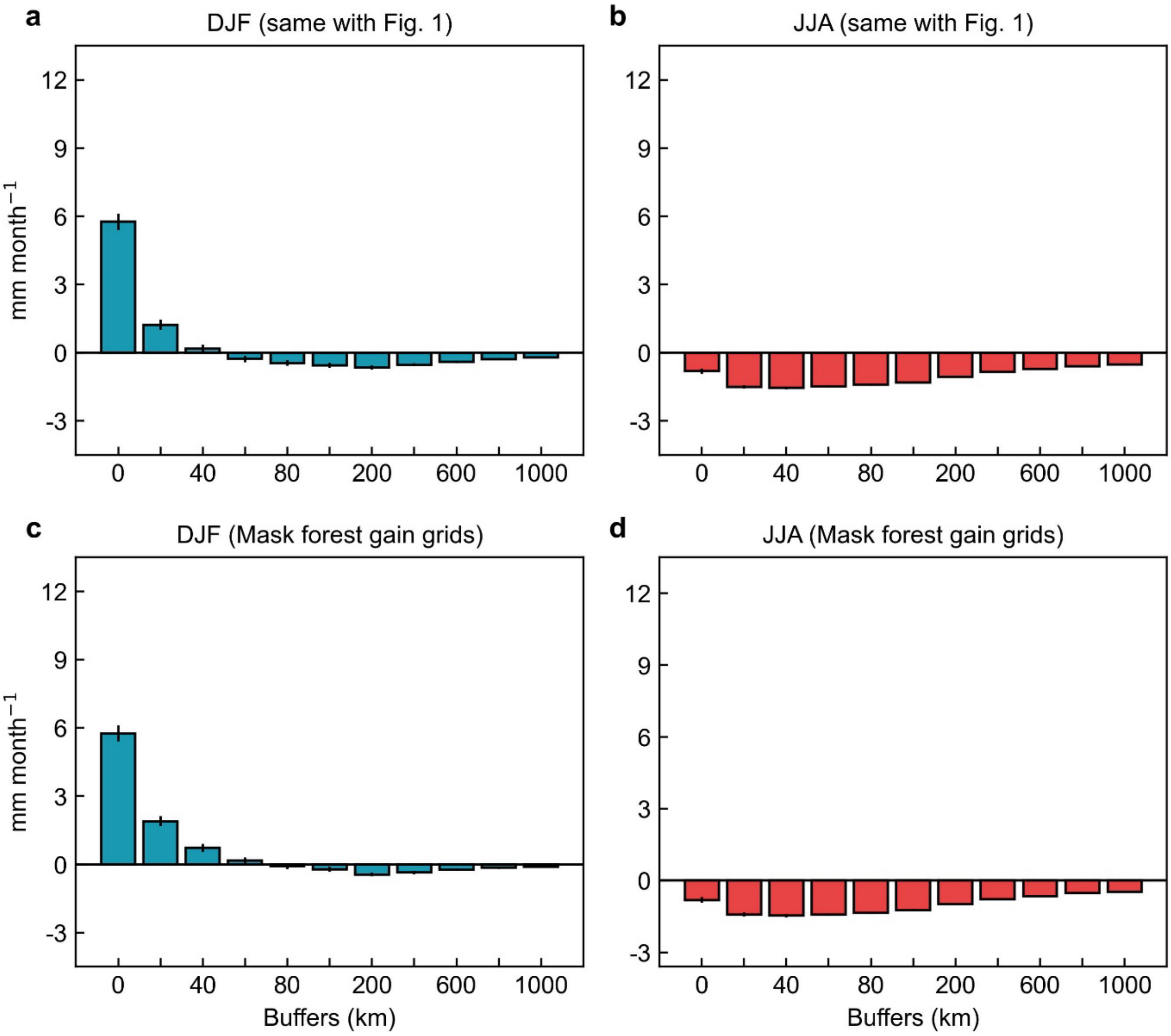

Figure S2. Comparisons of results with or without forest gain grids. a, b, Bars represent the mean ΔP of pixels in each buffer with different distances from deforested grids in DJF (a) and JJA (b). Error bars show ± standard error from the mean. **c, d**, Results excluding the forest gain grids (as shown in Extended Data Fig. 1).

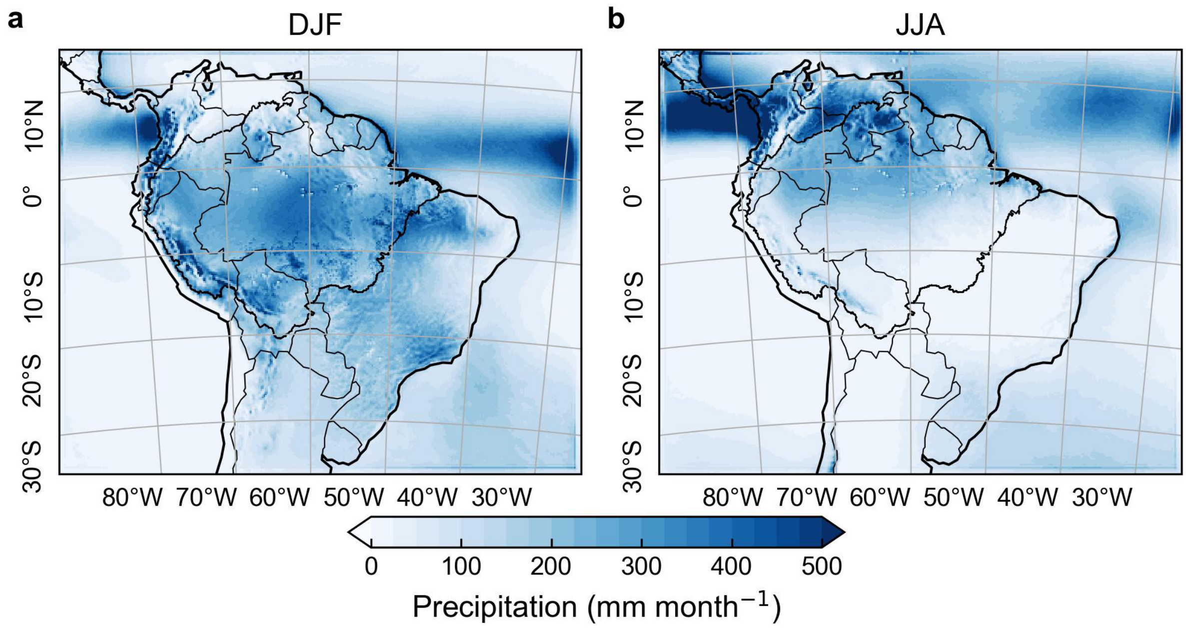

Figure S3. Simulated mean precipitation during the wet (a) and dry (b) seasons from 2001 to 2022.

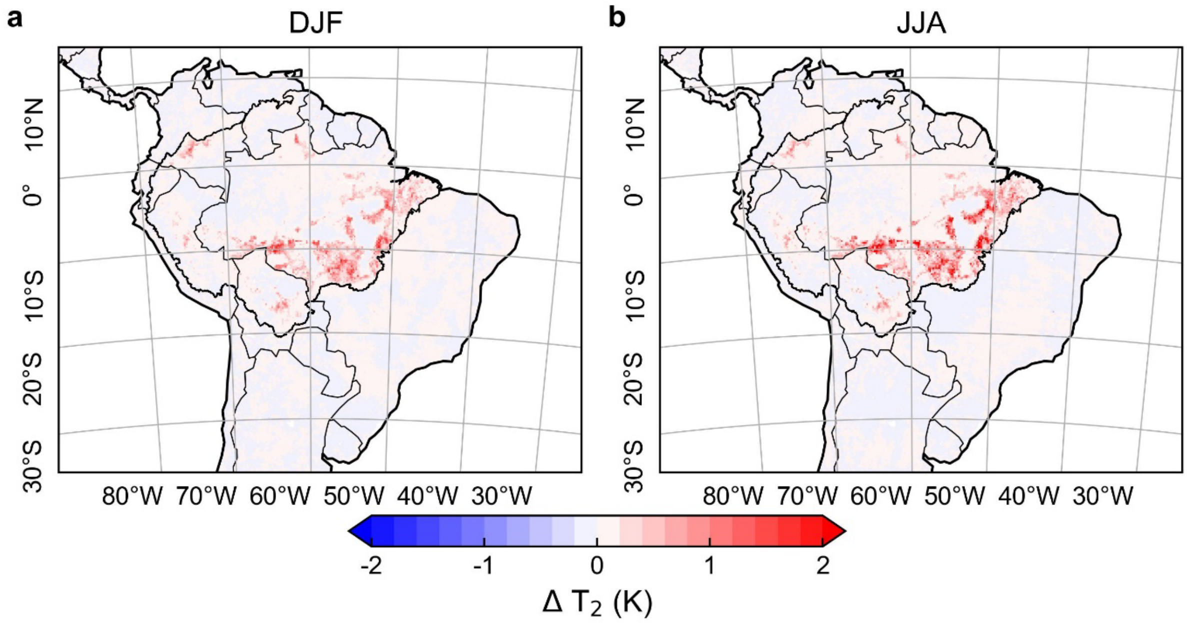

Figure S4. Simulated Amazon deforestation impacts on surface air temperature (2m). ΔT_2 ("S2020" minus "S2000") represents Amazon deforestation impacts on surface air temperature (2m) during the wet (a) and dry (b) seasons.

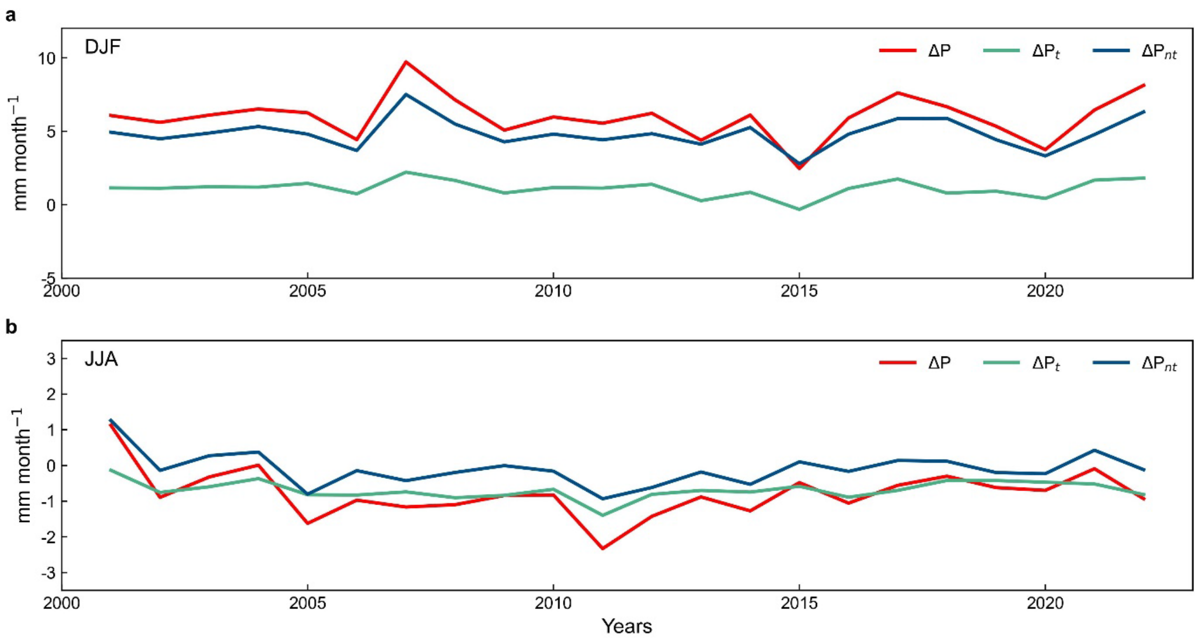

Figure S5. Interannual variability of precipitation effects of Amazon deforestation from 2001 to 2022. a, Precipitation effects of Amazon deforestation during the wet season (DJF). **b**, Precipitation effects of Amazon deforestation during the dry season (JJA).

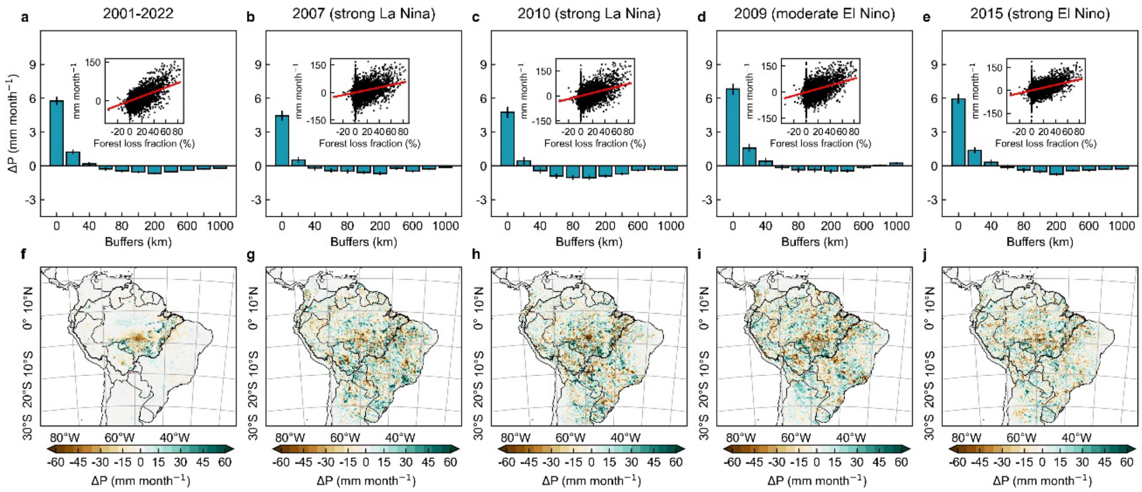

Figure S6. Comparisons of simulated precipitation impacts of Amazon deforestation during wet seasons under different climate forcing. a-e, Mean precipitation effects of each buffer with different distances from deforested grids under different climate forcing: 2001-2022 (a), 2007: strong La Niña (b), 2010: strong La Niña (c), 2009: moderate El Niño (d), 2015: strong El Niño (e). Error bars show ± standard error from the mean. **f-j**, Spatial patterns of precipitation changes under different climate forcing. Details of La Niña and El Niño years refer to: https://ggweather.com/enso/oni.htm.

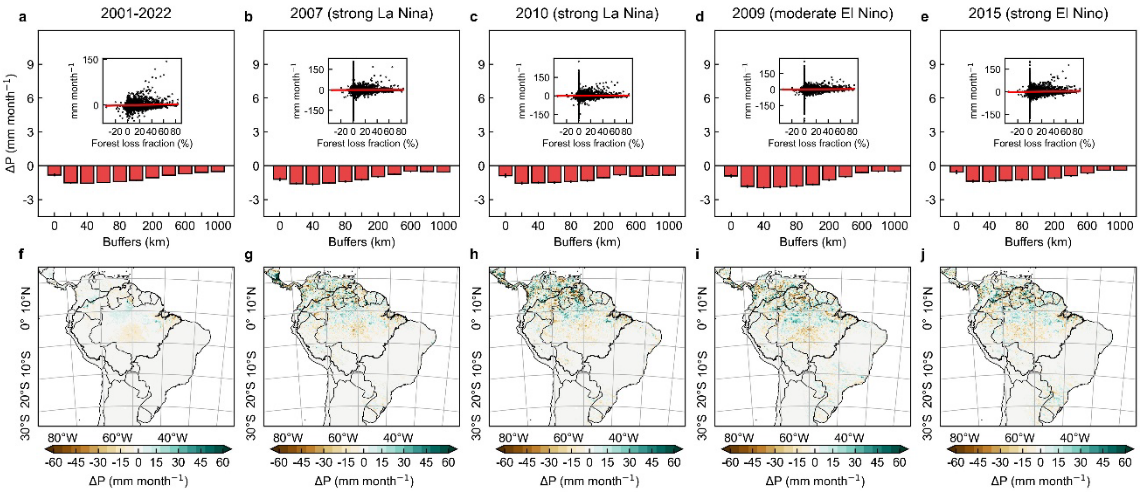

Figure S7. Comparisons of simulated precipitation impacts of Amazon deforestation during dry seasons under different climate forcing. a-e, Mean precipitation effects of each buffer with different distances from deforested grids under different climate forcing: 2001-2022 (a), 2007: strong La Niña (b), 2010: strong La Niña (c), 2009: moderate El Niño (d), 2015: strong El Niño (e). Error bars show ± standard error from the mean. **f-j**, Spatial patterns of precipitation changes under different climate forcing. Details of La Niña and El Niño years refer to: https://ggweather.com/enso/oni.htm.

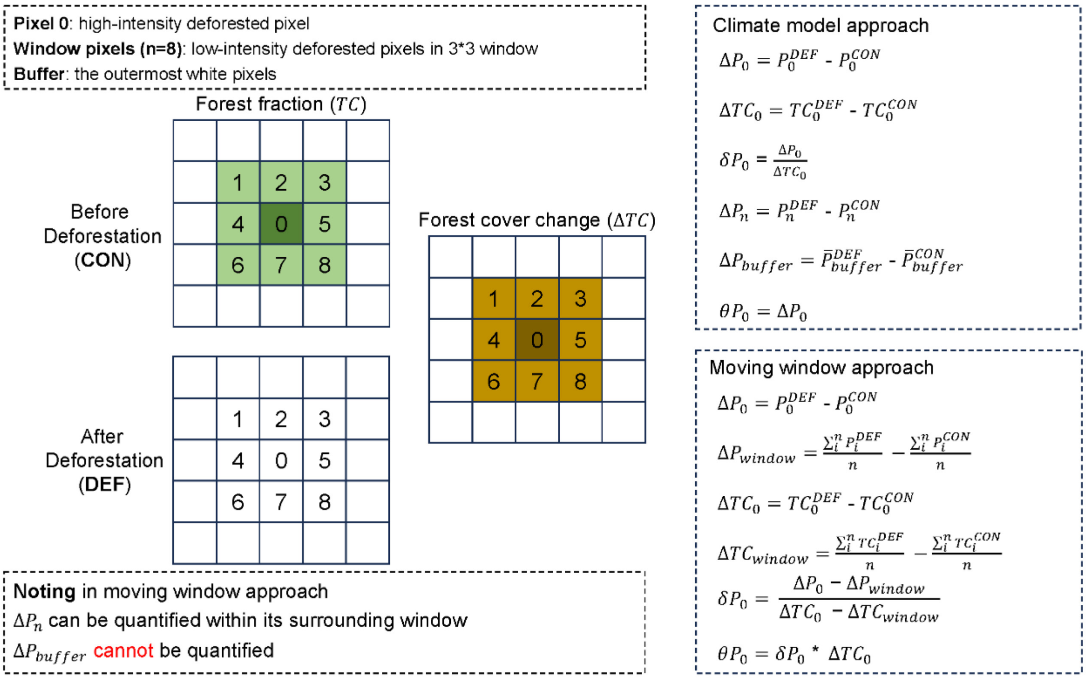

Figure S8. Comparisons between climate model and moving window approach in conceptual grids. Grid 0 is the deforested pixels whose precipitation impacts are needed to be quantified. Grids 1-8 are pixels surrounding grid 0 within a 3×3 window. Buffers in the climate model approach can be larger, as shown in buffer settings (Fig. S2). ΘP_0 represents precipitation impacts over deforested pixels in both approaches. ΘP_0 in the climate model approach can be easily quantified by precipitation in deforestation (DEF) scenario (P_0^{DEF}) minus control (CON) scenario (P_0^{CON}). Precipitation impacts of neighboring pixels (ΔP_n) and precipitation impacts on buffers (ΔP_{buffer}) can also be quantified by DEF minus CON. In the moving window approach, we need to derive precipitation changes (ΔP_0) and forest cover change (ΔTC_0) over the deforested grid 0 and surrounding window (ΔP_{window} and ΔTC_{window}) by DEF minus CON scenario. Precipitation sensitivity (δP_0) to deforestation can be quantified by comparing deforested grid 0 and neighboring grids. Finally, precipitation impacts (ΘP_0) can be quantified by the δP_0 multiplies tree cover change in grid 0 (ΔTC_0).

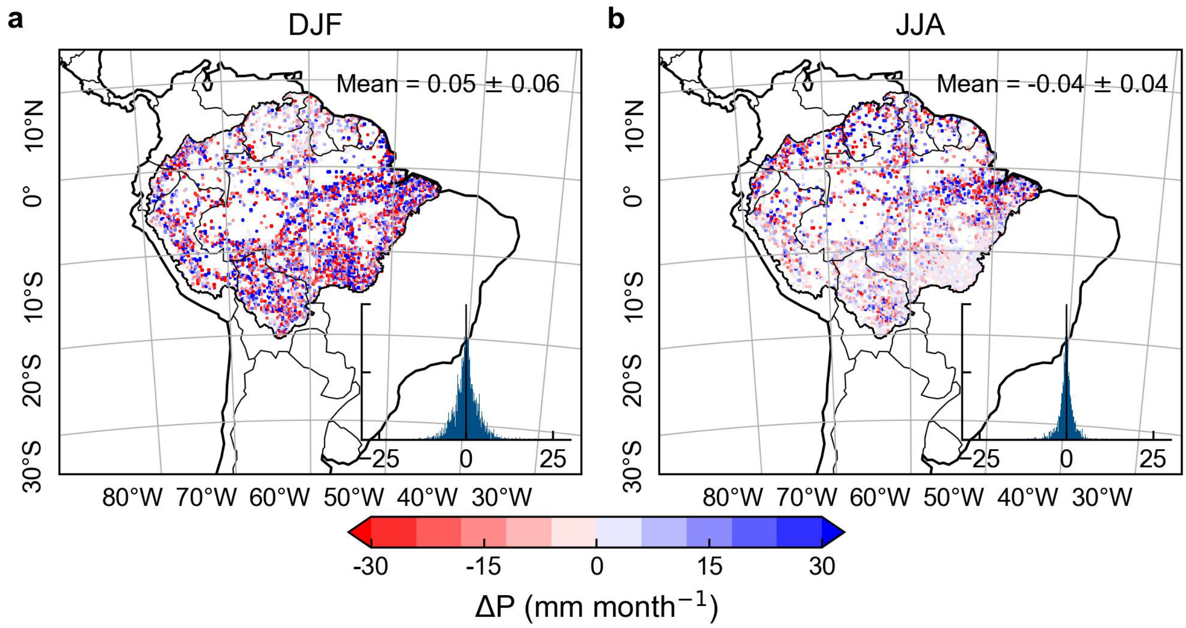

Figure S9. Satellite-based precipitation impacts induced by Amazon deforestation following method by Smith et al. (2023). Uncertainties show ± standard error from the mean. Inner figures show the distribution of precipitation effects during wet (a) and dry(b) seasons. 4 satellite rainfall datasets used in this analysis are detailed in Extended Data Table 1.

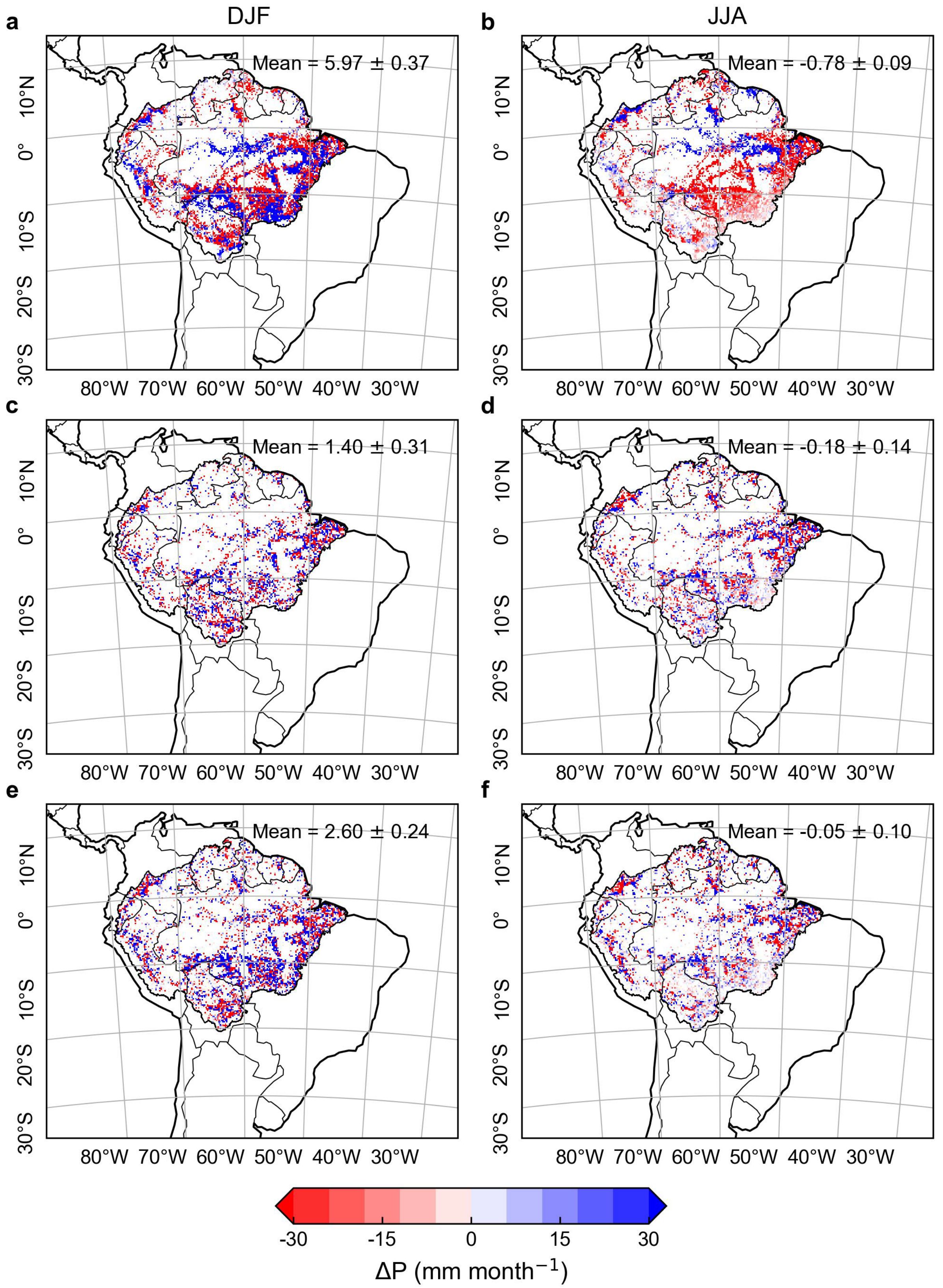

Figure S10. Precipitation impacts during the wet and dry seasons based on applying different methods to WRF simulations. a, **b,** Precipitation impacts quantified by experiment "S2020" minus "S2000" during the wet and dry seasons. **c, d**, Precipitation impacts quantified by applying binary-based moving window approach to WRF simulations during the wet and dry seasons. **e, f**, Precipitation impacts quantified by applying regression-based moving window approach to WRF simulations during the wet and dry seasons. Uncertainties show ± standard error from the mean. Details refer to the *Methods* part.

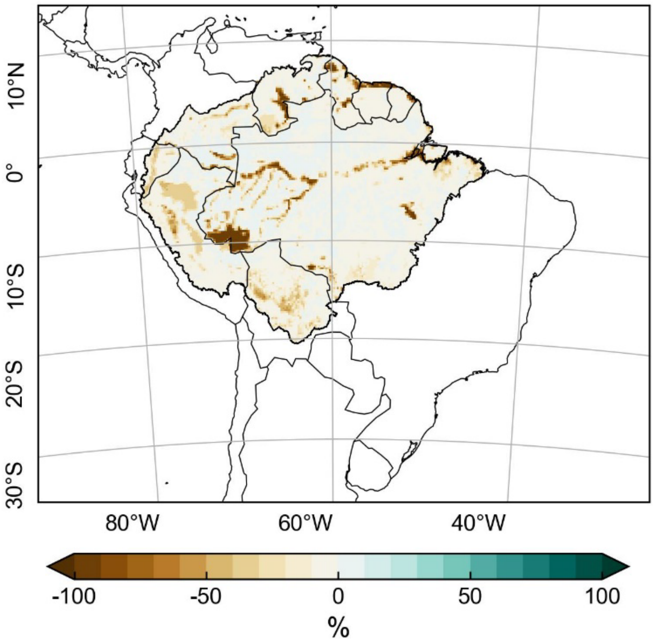

Figure S11. GCAM projected forest cover change (%) in the Amazon region from 2015 to 2100 under a regional rivalry scenario (SSP3-RCP4.5).

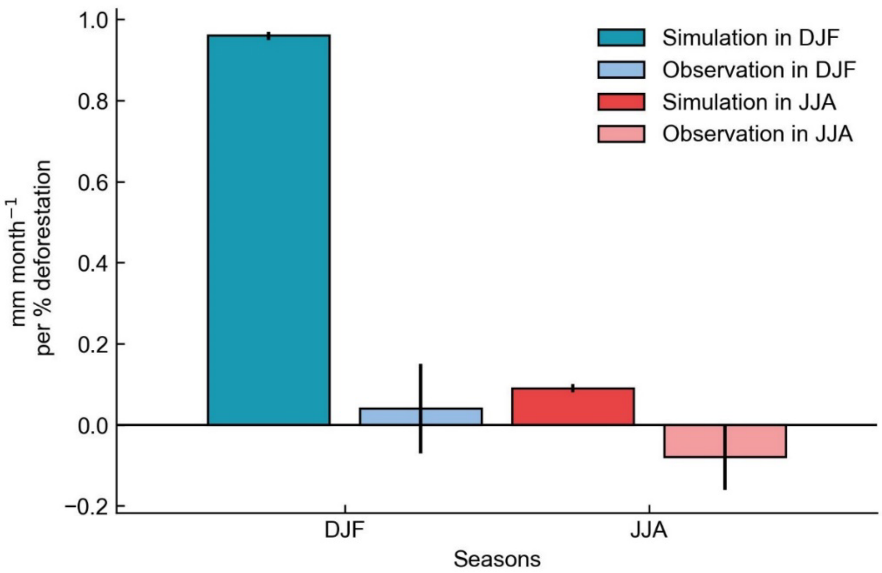

Figure S12. Comparisons of precipitation sensitivity to forest loss fraction over deforested pixels between simulation and satellite data. Satellite rainfall datasets used in this analysis are detailed in Extended Data Table 1. Error bars show ± standard error from the mean.

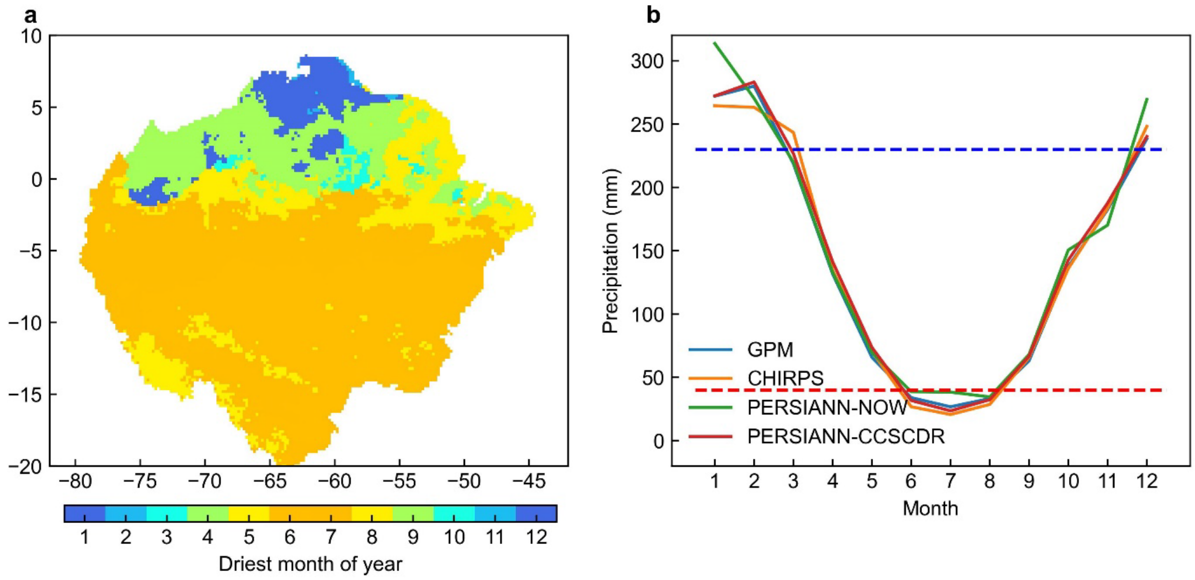

Figure S13. Monthly precipitation climatology over the Amazon region derived from satellite rainfall datasets. a, Driest month of the year derived from monthly mean precipitation of 4 rainfall datasets from 2000 to 2020. **b**, Monthly mean precipitation for the southern Amazon region (latitude between 10°S and 20°S). 4 satellite rainfall datasets used in this analysis are detailed in Extended Data Table 1. Blue and red dashed lines divide the wet and dry seasons over the Amazon region.

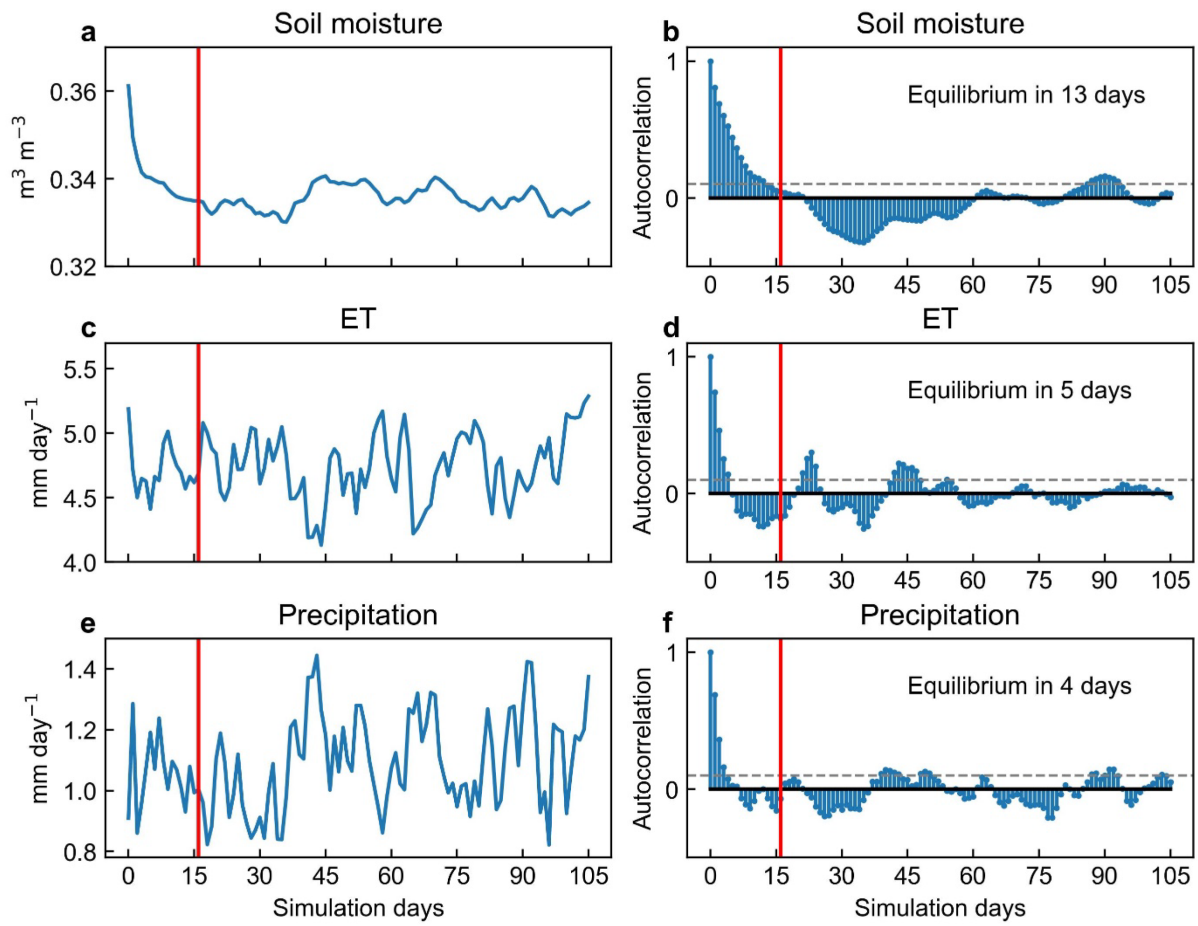

Figure S14. The evolution and equilibrium of simulations during the wet season in 2020. **a, b**, The evolution and equilibrium of soil moisture (averaged across 10 layers) are analyzed. Time series autocorrelation is employed to determine the point at which the time series reaches equilibrium (autocorrelation < 0.1), indicating when past conditions no longer significantly influence the current state. **c, d**, The evolution and equilibrium of ET. **e, f**, The evolution and equilibrium of precipitation. The red line marks the end of the initial 16-day spin-up period, distinguishing it from the subsequent 3-month simulation period used for analysis. The gray dashed line marks the autocorrelation function is less than 0.1.

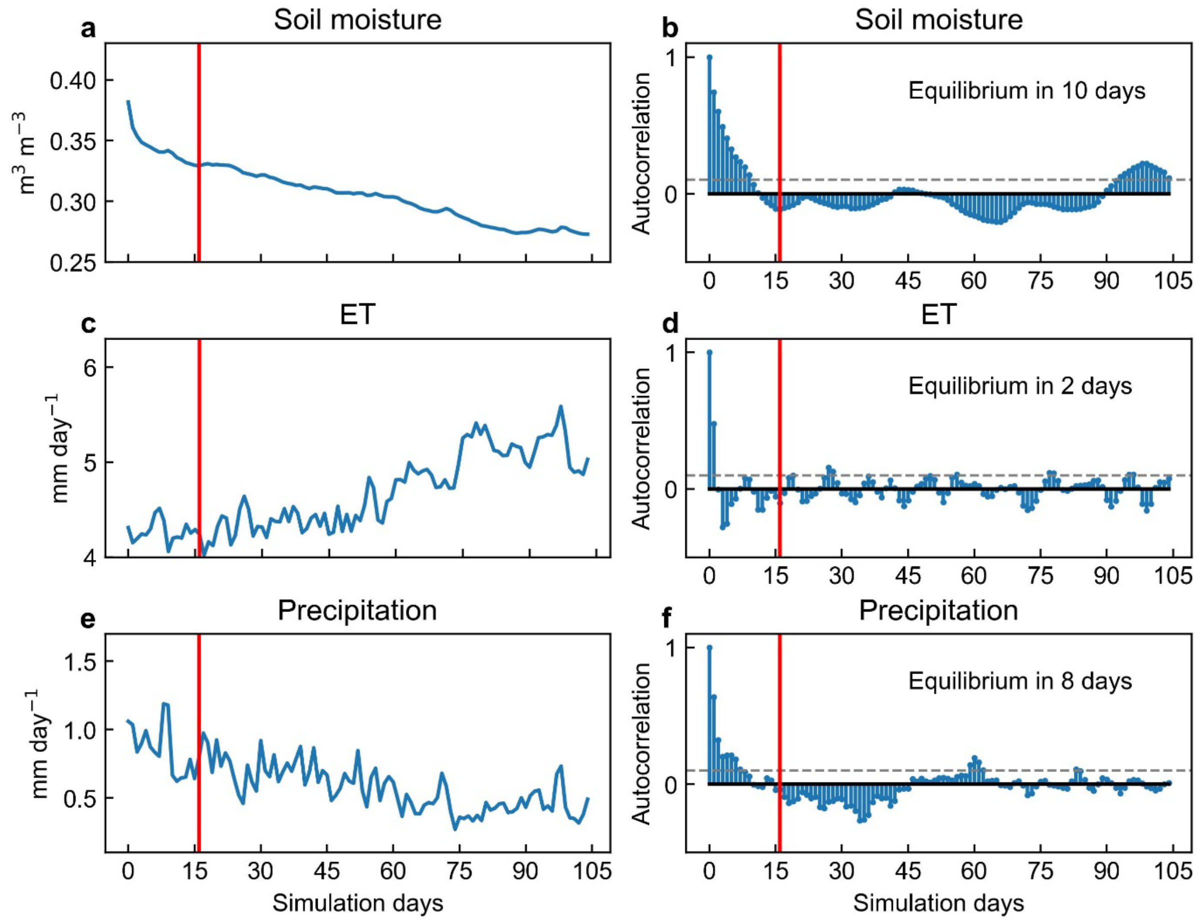

Figure S15. The evolution and equilibrium of simulations during the dry season in 2020. **a, b**, The evolution and equilibrium of soil moisture (averaged across 10 layers) are analyzed. During the dry season, soil moisture continues to decrease owing to the drought stress. It is time series autocorrelation that is used to determine the point at which the time series reaches equilibrium (autocorrelation < 0.1), indicating when past conditions no longer significantly influence the current state. **c, d**, The evolution and equilibrium of ET. **e, f**, The evolution and equilibrium of precipitation. The red line marks the end of the initial 16-day spin-up period, distinguishing it from the subsequent 3-month simulation period used for analysis. The gray dashed line marks the autocorrelation function is less than 0.1.

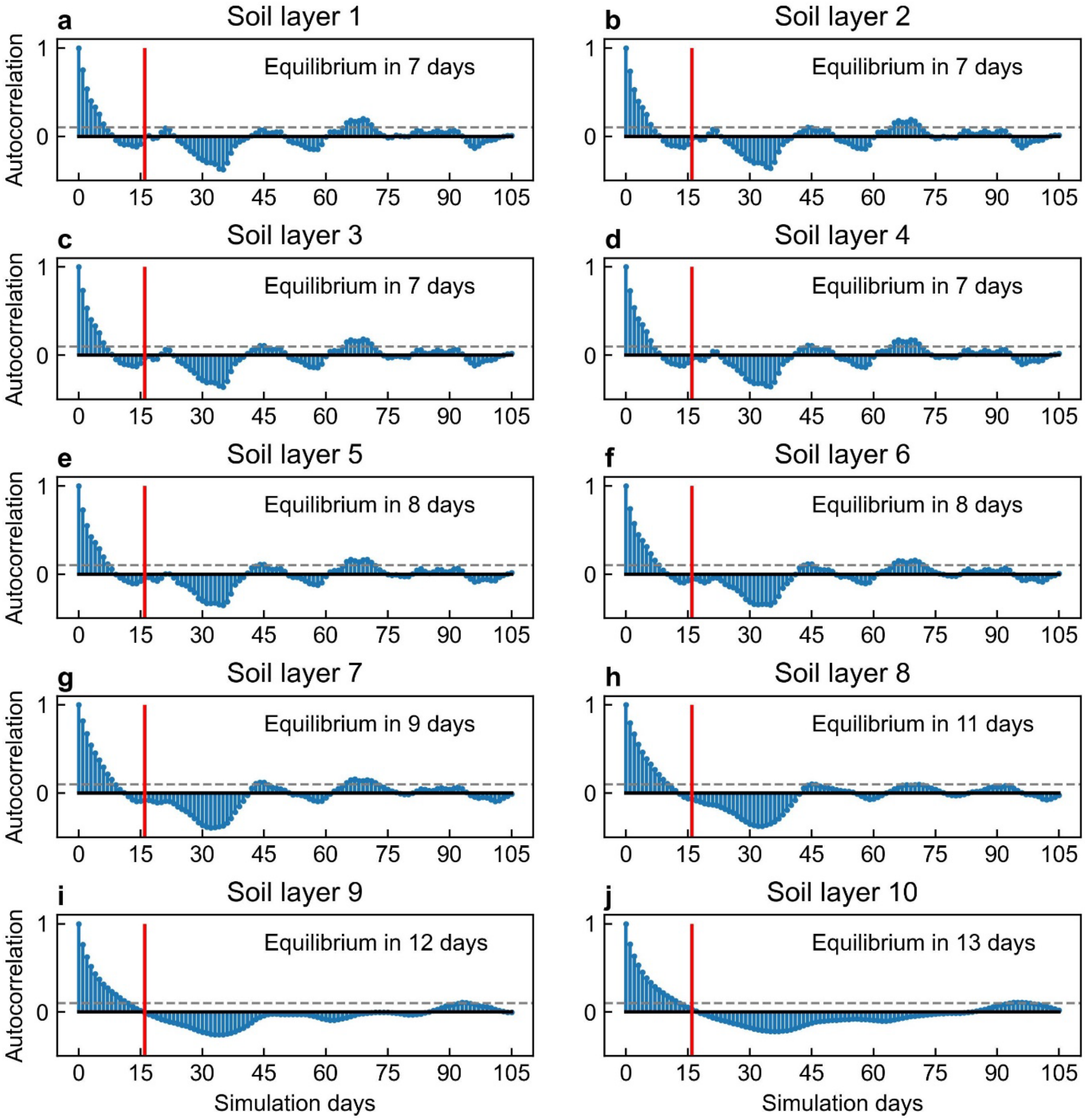

Figure S16. Time series autocorrelation used to assess the equilibrium of soil moisture across different layers during the wet season in 2020. The ten soil layers in CLM are represented in panels a-j. The red line marks the end of the initial 16-day spin-up period, distinguishing it from the subsequent 3-month simulation period used for analysis. The gray dashed line marks the autocorrelation function is less than 0.1.

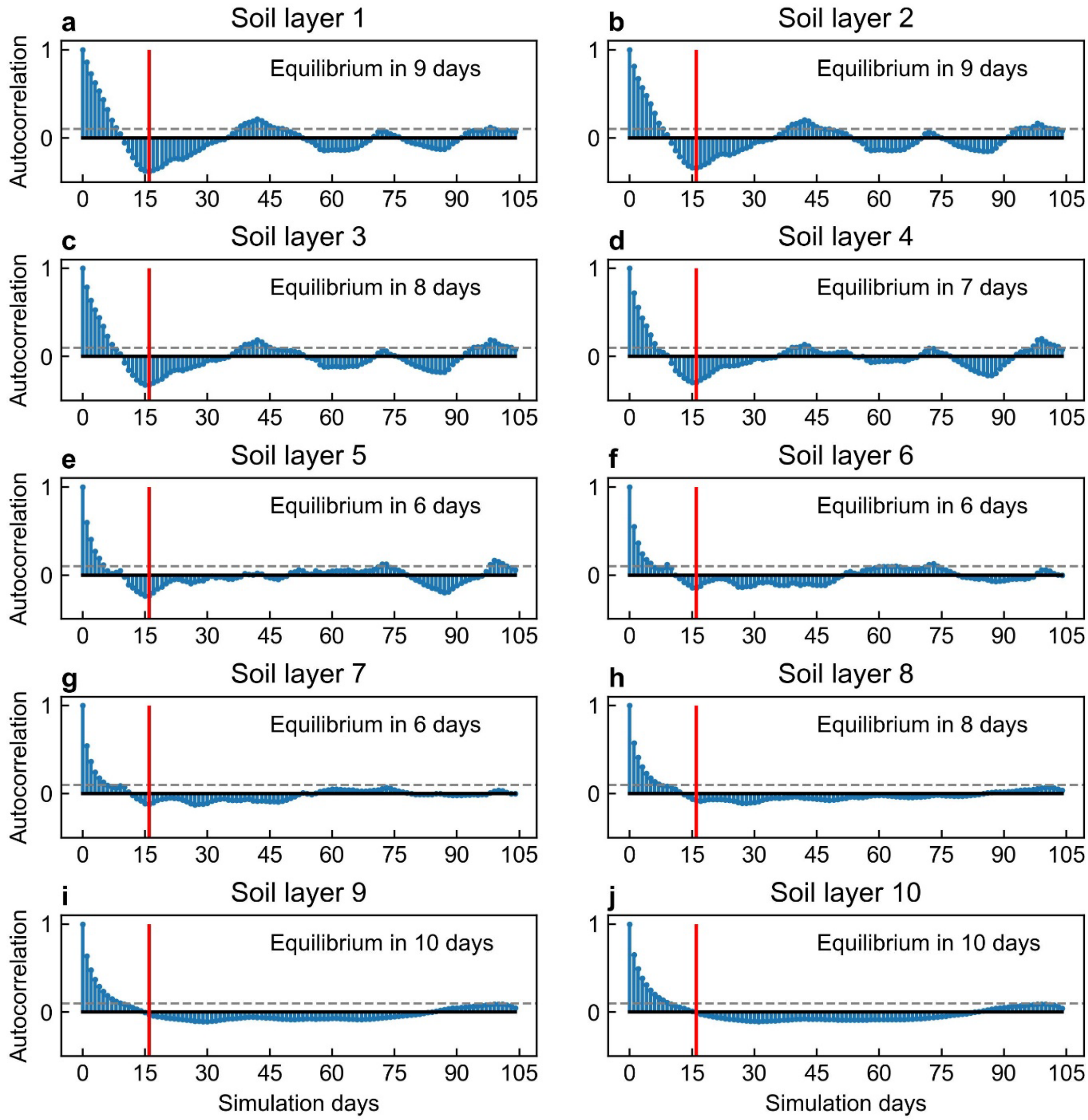

Figure S17. Time series autocorrelation used to assess the equilibrium of soil moisture across different layers during the dry season in 2020. The ten soil layers in CLM are represented in panels a-j. The red line marks the end of the initial 16-day spin-up period, distinguishing it from the subsequent 3-month simulation period used for analysis. The gray dashed line marks the autocorrelation function is less than 0.1.